analytical chemistry

Article

pubs.acs.org/ac

High-Efficient Energy Funneling Based on Electrochemiluminescence Resonance Energy Transfer in Graded-Gap Quantum Dots Bilayers for Immunoassay

Jing Ji, Li He, Yuanyuan Shen, Pingping Hu, Xinghua Li, Li-Ping Jiang, Jian-Rong Zhang, Lingling Li,* and Jun-Jie Zhu*

State Key Laboratory of Analytical Chemistry for Life Science, School of Chemistry and Chemical Engineering, Nanjing University, Nanjing 210093, P. R. China

Supporting Information

ABSTRACT: A surprising electrochemiluminescence (ECL) enhancement effect in graded-gap CdSeTe@ZnS-SiO_2 quantum dot (QD) bilayers was observed and used to create an ultrasensitive immunoassay. CdSeTe@ZnS-SiO_2 QDs of two different sizes were used as a donor−acceptor pair, owing to their tunable energy and low biotoxicity. The graded-gap CdSeTe@ZnS-SiO_2 QD bilayers were fabricated by layer-by-layer assembly of differently sized CdSeTe@ZnS-SiO_2 QDs on a glutaraldehyde-activated electrode. Benefiting from a short interlayer distance and perfect spectral overlap in the graded-gap QD bilayers, highly efficient ECL resonance energy transfer (ECLRET)-based energy funneling was observed, wherein excitons from trapped states could be effectively recycled. Consequently, the observed ECL enhancement for the bilayers was more than four times greater than that observed for reference samples. The graded-gap QD bilayers were utilized in an ECL biosensor for the detection of carcinoembryonic antigen (CEA). The proposed method featured a detection limit of 0.4 pg mL^{-1} CEA with a linear calibration range from 1 pg mL^{-1} to 200 ng mL^{-1}. This method represents a novel approach for versatile detection of biomolecules in research and clinical applications.

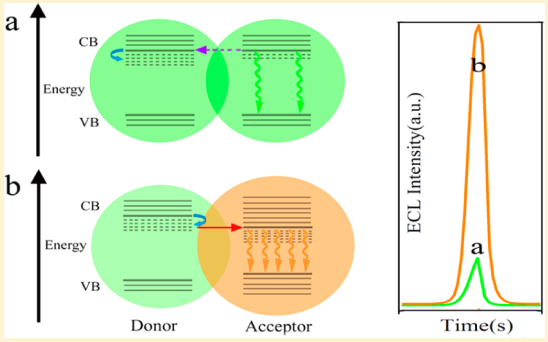

Fluorescence resonance energy transfer (FRET) is a type of nonradiative energy transfer mechanism that can occur between a suitably matched acceptor and donor pair. The efficiency of the FRET process is determined by overlapping integrals of the excitation and emission spectra as well as the orientation and distance between the donor and acceptor label.[1] Studies of FRET have been reported using fluorescent dyes or proteins and quantum dots (QDs).[2−9] However, because FRET requires external illumination to initiate the fluorescence transfer, background noise is often incurred. To avoid this drawback, resonance energy transfer systems based on other forms of luminescence have been developed, such as those based on bioluminescence, chemiluminescence, and electrochemiluminescence.[10−12] Among them, electrochemiluminescence (ECL), chemiluminescence triggered by electrochemical methods via a redox reaction of electrogenerated reactants, has attracted increasing interest.[13−16] ECL combines the electrochemical and luminescent techniques and exhibits its unique advantages, such as the absence of background arising from nonselective photoexcitation, high sensitivity, wide dynamic concentration response range, and its potential and spatial control.[17] Thus ECL technique has been widely used in various fields, ranging from theory study to biosensors for the detection of small molecules, proteins, DNA, cells, etc.[18−22] For these reasons, electrochemiluminescence resonance energy transfer (ECLRET), which occurs based on the overlap of the ECL spectrum of the ECL species with the absorption spectrum of the acceptor, is a promising approach for further study of energy transfer.

Despite the aforementioned advantages, little attention has been paid to ECLRET because it is difficult to identify a suitable donor−acceptor pair.[12] With consideration of the increasing numbers of reports on QD ECL,[23−26] QDs are especially appealing as potential donors and acceptors, since their optical properties can be tailored to meet specific wavelength requirements by simply changing their chemical composition or size.[27] Thus, QD-based ECLRET is an effective method for electrochemical analysis.[28]

Apart from the abundant studies on QDs in solution for efficient FRET-based sensors,[29] FRET investigation of solid-state QD-based systems holds much promise for the creation of novel light harvesters. More specifically, much attention has been given to multilayered QD structures, for which precisely controlled energy gap gradients can be induced by sequentially varying the sizes or compositions of the QDs among the

Received: July 23, 2013
Accepted: February 27, 2014
Published: February 27, 2014

   dx.doi.org/10.1021/ac500351d | Anal. Chem. 2014, 86, 3284−3290

layers.[30−32] FRET cascades from large bandgap QDs to smaller bandgap QDs allow greatly improved energy transfer rates and power conversion efficiencies to be obtained from this kind of graded-gap, multilayered QD structure (as shown in Figure 4B).[4,33,34] In addition, the luminescence color of the resulting films can be easily tuned by changing the QDs size, assembly sequence, and deposition cycle number to control the FRET degree.[30,31] It is particularly noticeable that surprisingly intense photoluminescence, with wavelength corresponding to that of the smallest bandgap QDs, was yielded in the graded-gap QDs multilayers, which was over four times higher than a reference sample consisting of equal layers of the narrowest bandgap QDs.[35,36] The recycling of trapped and lost excitons and the avoidance of hot carriers via stepwise passing on of excitation energy were considered mainly responsible for the fluorescence enhancement effect. These results render graded-gap QD multilayers promising for the development of high-performance solar cells, multicolored-light-emitting diodes, and optical sensors. Accordingly, inspired by this fluorescence enhancement effect, one can expect that greatly enhanced ECL signals may also be obtained in the graded-gap QD multilayers. At present, some groups have studied energy transfer between QDs and organic molecules, nanorods, and other kinds of nanoparticles.[7,37−40] However, as far as we know, the study on ECLRET in graded-gap QDs multilayers has not been reported.

Herein, we explored the ECLRET properties in CdSeTe@ZnS-SiO_2 QD (QDs with a CdSeTe core and a SiO_2 shell filled with ZnS-like clusters) bilayers and developed a novel ECL immunosensor for CEA detection. Graded-gap QD bilayers were fabricated by layer-by-layer assembly of two differently sized QDs on the glutaraldehyde-activated electrode, as shown in Scheme 1. The resulting tiny interlayer distance and excellent spectral overlap between these two QDs ensured a high ECLRET efficiency, and as a result, a greatly enhanced ECL signal was obtained, which was more than four times higher than that obtained from the bilayer reference samples containing only one type of QD. The QD bilayer configuration was applied to fabricate an ECL immunosensor for the determination of carcinoembryonic antigen (CEA). The stability, reproducibility, and accuracy of the immunosensor were also investigated. This investigation indicated that the ECLRET in QD multilayers had a wide range of potential applications in clinical and molecular diagnostics.

Scheme 1. Fabricating Steps of the QD Bilayers and Corresponding ECL Immunosensor

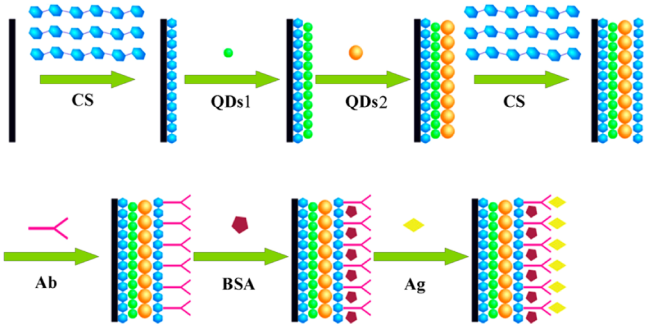

EXPERIMENTAL SECTION

Chemicals and Materials. CEA (Ag), anti-CEA (Ab), and complementary CEA ELISA kit were purchased from Shanghai Linc-Bio Science Company Ltd. BSA (96−99%) was obtained from Sigma-Aldrich Chemical Company (St. Louis, MO); glutaraldehyde solution (25%) was obtained from Sinopharm Chemical Reagent Company, Ltd. (Shanghai, China), and chitosan was obtained from Nanjing DeBioChem Company, Ltd. (Nanjing, China). Ultrapure water obtained from a Millipore water purification system (≥18 MΩ, Milli-Q, Millipore) was used in all assays. All other reagents were of analytical grade and were used as received without further purification. Phosphate-buffered saline (PBS) with various pH values was prepared by mixing stock solutions of NaH_2PO_4 and Na_2HPO_4 and then adjusting the pH with 0.1 M NaOH and H_3PO_4. The washing buffer was PBS (0.01 M, pH 7.4) containing 0.05% (w/v) Tween 20 (PBST). The blocking solution was PBS (0.01 M, pH 7.4) with 1% (w/v) BSA. A solution of 0.05 M PBS (pH 7.4) containing 0.1 M $K_2S_2O_8$ and 0.1 M KCl was used as the electrolyte in ECL analysis. A solution of 0.01 M PBS (pH 7.4) containing 1.0 mM $K_3Fe(CN)_6$ and 0.1 M KCl was used for cyclic voltammetry (CV) measurements. A solution of 0.01 M PBS (pH 7.4) containing 2.5 mM $[Fe(CN)_6]^{3-/4-}$ and 0.1 M KCl was used for electrochemical impedance spectroscopy (EIS) measurements.

Apparatus. The ECL intensity was detected with a model MPI-A Electrochemiluminescence Analyzer (Xi'An Remax Electronic Science & Technology Company Ltd., Xi'An, China) with a conventional three-electrode system composed of a platinum wire as the auxiliary electrode, a saturated calomel electrode (SCE) as the reference, and bare or modified glassy carbon electrodes (GCE, 4 mm diameter) as working electrodes. The emission window was placed in front of a photomultiplier tube (PMT) biased at 600 V. The ECL spectra were obtained by collecting the ECL peak intensity during the cyclic potential sweep with a series of optical filters at 400, 450, 470, 510, 535, 565, 580, and 600 nm. UV−vis spectra were recorded on a UV-3600 spectrophotometer (Shimadzu, Kyoto, Japan). Photoluminescence (PL) spectra were obtained on a RF-5301PC spectrophotometer (Shimadzu, Kyoto, Japan). Atomic force microscopy (AFM) images were obtained on a SPI3800 controller operated in tapping mode with an acquisition frequency of 1.5 Hz and a line density of 512.2 × 2 μm scans.

Synthesis of QDs. CdSeTe@ZnS-SiO_2 quantum dots of two different sizes were synthesized under microwave irradiation for 20 and 50 min;[41] we refer to these QDs herein as QDs1 and QDs2, respectively. Glutathione was employed as the capping agent to stabilize the QDs and to provide amino groups for the immobilization of the QDs. The existence of amino group on the QDs surface was validated by FT-IR spectra (Figure S1 of the Supporting Information). The QDs were purified through ultrafiltration under centrifugation (3000 MW, 3000 rpm).

Preparation of QD Bilayers. As shown in Scheme 1, a chitosan (CS) solution (0.1% w/v, 10 μL) was dropped onto a pretreated GCE and allowed to dry at room temperature. Then, glutaraldehyde solution (5% w/v, 10 μL) was dropped onto the electrode and allowed to dry for 30 min. After rinsing thoroughly with water, the electrode was quickly dried with N_2. Then 10 μL of QDs1 was dropped onto the electrode and dried in air to obtain a QDs1 layer. This same process was repeated using glutaraldehyde followed by QDs2 solution, to finally yield a QD-bilayer-modified GCE. After air-drying the modified electrode, CS solution (0.1% w/v, 10 μL) was then

dx.doi.org/10.1021/ac500351d | Anal. Chem. 2014, 86, 3284−3290

dropped onto the QD-bilayer-modified GCE to cover the modified surface. Two reference samples comprising two monolayers of only QDs1 or QDs2 were also prepared following the same procedure.

Preparation of the ECL Immunosensor. To prepare the ECL immunosensor for CEA detection, glutaraldehyde solution (5% w/v, 10 μL) was dropped onto the modified GCE for 30 min. After thoroughly washing, the GCE was immersed in 10 μg mL^{-1} rat anti-CEA (Ab) solution (10 mM PBS, pH 7.4, 50 μL) at 4 °C overnight. Then, the GCE was rinsed with pH 7.4 PBST to remove physically adsorbed proteins and incubated in 50 μL of 1 wt % BSA at 37 °C for 30 min to block nonspecific binding sites. After rinsing again with pH 7.4 PBST, the modified GCE was immersed in 50 μL of CEA (Ag) samples with different concentrations at 37 °C for 1 h. Finally, the electrode was rinsed with PBST. The resulting electrode was stored in the refrigerator at 4 °C when not in use.

ECL Detection. The modified electrodes were in contact with 0.05 M PBS (pH 7.4) containing 0.1 M $K_2S_2O_8$ and 0.1 M KCl and scanned from 0 to −1.5 V with a scan rate of 200 mV s^{-1}. ECL signals related to the CEA concentrations were measured.

RESULTS AND DISCUSSION

Characterization of the Graded-Gap QD Bilayers. To fabricate the graded-gap QD bilayers, two differently sized CdSeTe@ZnS-SiO_2 QDs were selected by varying the reaction time used for QD synthesis. The smaller QDs (QDs1), which had an average diameter of 4.8 nm, were used as the donor and emitted green light, whereas the larger QDs (QDs2), which had average diameters of 5.2 nm, were used as the acceptor and emitted orange light.[41] Scheme 1 illustrates the fabrication process of the graded-gap QD bilayer films. The QDs were conjugated to glutaraldehyde-activated chitosan on the GCE in a sequence from smaller to larger sizes. Due to the quantum confinement effect, the conduction band (CB) and valence band (VB) energies of the QDs are strongly size-dependent, and thus a layer sequence with gradual changing of QD diameters created an intrinsic ramp of hole and electron potentials.

The degree of spectral overlap between the donor and acceptor is of great importance for resonance energy transfer, with better overlap providing higher transfer efficiency.[42] Herein, by varying the sizes of the QDs, two kinds of QDs were obtained with optimal spectral overlap. Figure 1 shows the PL, UV−vis absorption, and ECL spectra of QDs1 and QDs2. The typical absorption peaks of QDs1 (Figure 1A, red dotted line) and QDs2 (Figure 1A, blue dotted line) are observed at 516 and 556 nm. The change in the absorption maximum confirmed the decrease in the band gap from QDs1 to QDs2. The PL emission peaks of the QDs were at 556 nm (Figure 1A, red solid line) and 591 nm (Figure 1A, blue solid line), respectively. In other words, the absorption spectrum of QDs2, as the acceptor, overlapped perfectly with the emission spectrum of the donor, QDs1, thus ensuring that resonance energy transfer would occur. Figure 1B shows the normalized ECL spectra of QDs1 and QDs2 with a maximum wavelength at 550 nm (red line) and 588 nm (blue line), respectively, which are aligned with their PL spectra.

Apart from the degree of spectral overlap, the transfer efficiency is still strongly dependent on the separation distance between the acceptor and donor.[42] Atomic force microscopy (AFM) was used to measure the modified QD films.

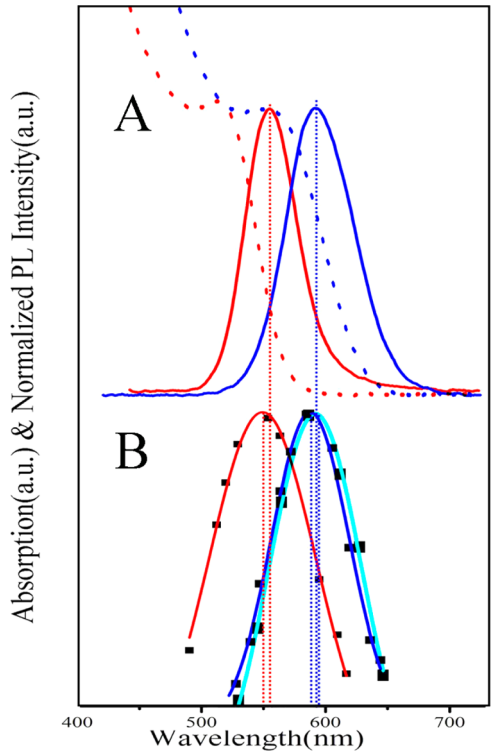

Figure 1. (A) UV−vis absorption spectra (dotted lines) and normalized PL spectra (solid lines) of CdSeTe@ZnS-SiO_2 QDs. (B) ECL spectra of CdSeTe@ZnS-SiO_2 QDs (red line is QDs1, blue line is QDs2, and cyan line is CS/QDs1/QDs2/CS).

As shown in Figure 2, the prepared QDs1 film was a homogeneous thin film with an average thickness of about 7.5 nm. Taking into consideration the contribution of CS layer to the overall thickness (Figure S2 of the Supporting Informa-

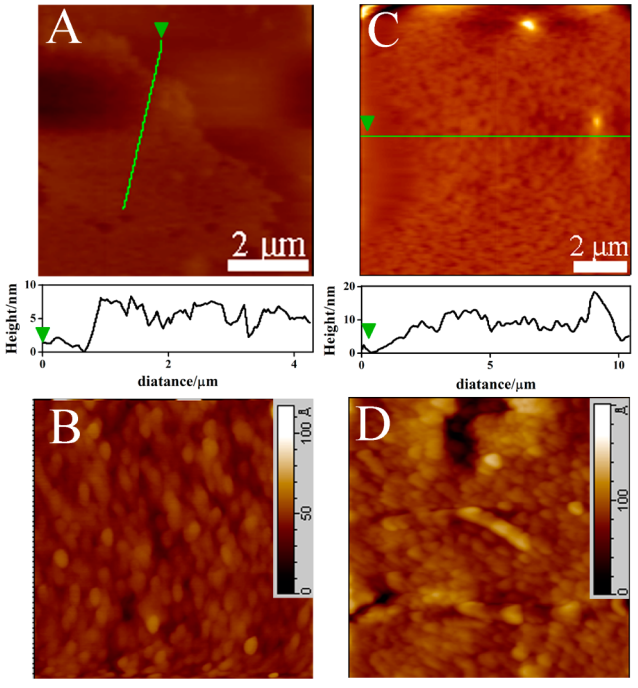

Figure 2. (A and B) AFM images of QDs1 monolayer and (C and D) QDs1/QDs2 bilayers.

dx.doi.org/10.1021/ac500351d | Anal. Chem. 2014, 86, 3284−3290

tion), the QDs1 film consisted of a uniformly distributed monolayer of QDs. After a QDs2 film was prepared on top of the QDs1 film, the measured thickness was 13.3 nm, suggesting that the QDs2 layer was also a monolayer. Owing to covalent connection between the glutaraldehyde-activated capping amine groups, the QDs2 monolayer was in very close proximity to the QDs1 monolayer, thus promoting high transfer efficiency.

ECL Behavior of the Graded-Gap QD Bilayers. The ECL spectrum of the graded-gap QD bilayers is shown in Figure 1B (cyan line). Clearly, only an emission peak at 592 nm ascribed to QDs2 is discernible, and the emission corresponding to QDs1 is suppressed. This indicates that ECLRET between QDs1 and QDs2, namely energy transfer from the higher-band gap QDs1 to the lower-band gap QDs2, was highly efficient. The key to such high-energy transfer efficiency is the perfect spectral overlap between QDs1 and QDs2, as well as their tiny interlayer distance.

The ECL-potential curves of different modified electrodes are shown in Figure 3. ECL peaks are observed at −1.49 V for the QDs1 layer (curve b) and at −1.47 V for the QDs2 layer (curve c), suggesting again that QDs2 had a smaller band gap than that of QDs1. An intense ECL signal was observed for the QDs1/QDs2 bilayers (curve f), which is about six times higher than that observed from either QD monolayer. For comparison, two reference samples comprising only a QDs1 bilayer or a QDs2 bilayer were fabricated and their ECL curves are shown in Figure 3 (curves d and e). Surprisingly, the ECL signal obtained from the graded-gap QD bilayers is more than four times higher than that obtained from the reference samples containing only one type of QD. This striking ECL enhancement effect in the graded-gap bilayer film is probably attributable to the ECLRET between QDs1 and QDs2, which will be further discussed in the next section.

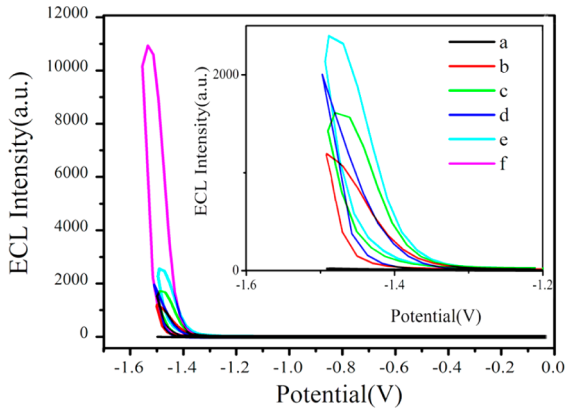

Figure 3. ECL-potential curves of modified electrodes: (a) bare GCE, (b) CS/QDs 1/CS/GCE, (c) CS/QDs2/CS/GCE, (d) CS/QDs1/QDs1/CS/GCE, (e) CS/QDs2/QDs2/CS/GCE, and (f) CS/QDs2/QDs1/CS/GCE. The inset are the enlarged ECL− potential curves of (a−e).

In accordance with previous reports, the ECL behavior of CdSeTe@ZnS-SiO_2 is similar to that of other QDs, such as CdSe and carbon nanocrystals.[43,44] Consequently, the ECL mechanism of CdSeTe@ZnS-SiO_2 QDs is proposed as follows: first, strongly oxidizing $SO_4^{\bullet-}$ radicals and $QD^{\bullet-}$ radicals are produced by electrochemical reduction of $S_2O_8^{2-}$ and QDs. Then, $SO_4^{\bullet-}$ radicals can react with $QD^{\bullet-}$ to emit light in the aqueous solution by producing an excited state (QD*). The possible ECL mechanisms are described with the following equations:

$$QDs + ne^- \rightarrow nQDs^{\bullet-} \quad (1)$$

$$S_2O_8^{2-} + e^- \rightarrow S_2O_8^{\bullet 2-} \quad (2)$$

$$S_2O_8^{\bullet 2-} \rightarrow SO_4^{2-} + SO_4^{\bullet-} \quad (3)$$

$$QDs^{\bullet-} + SO_4^{\bullet-} \rightarrow QDs^* + SO_4^{2-} \quad (4)$$

$$QDs^* \rightarrow QDs + h\nu \quad (5)$$

Insights into the ECL Enhancement Effect. The theoretical mechanism of FRET, particularly the PL enhancement, between graded-gap QD multilayers has been demonstrated.[33,35,45,46] These theories also hold for ECLRET in the structures studied here. Accordingly, we propose a mechanism for the observed high ECL enhancement in Figure 4. In films of closely packed QDs, most of the excited electron−hole pairs (98%) decay nonradiatively via defect states, whereas only 2% of the excited electron−hole pairs contribute to radiative emission.[7] In addition, the number of defects per nanocluster reportedly varies quite drastically. Therefore, in the excited reference samples, taking the QDs1 bilayers as an example (Figure 4A), most of the excitons in defect-rich QDs are effectively captured in nonluminescent surface traps (indicated by the blue curved arrow) and then decay nonradiatively. It is likely that only a few excitons in defect-poor QDs decay radiatively (green arrows); however, these excitons could also be captured by nearby defect-rich QDs (purple arrow) and then be trapped. For the graded-gap QDs1/QDs2 bilayers, not only could radiative excitons be transferred from QDs1 to QDs2 based on resonant energy transfer, but trapped excitons could also be resonantly transferred to luminescent states of nearby QDs2 and thereby be recycled (red arrow). Notably, the recycled excitons had only little excess energy and were therefore less prone to be retrapped. The observed lack of ECL emission from the QDs1 layer in the QDs1/QDs2 bilayers supports this interpretation. In summary, the recycling of the

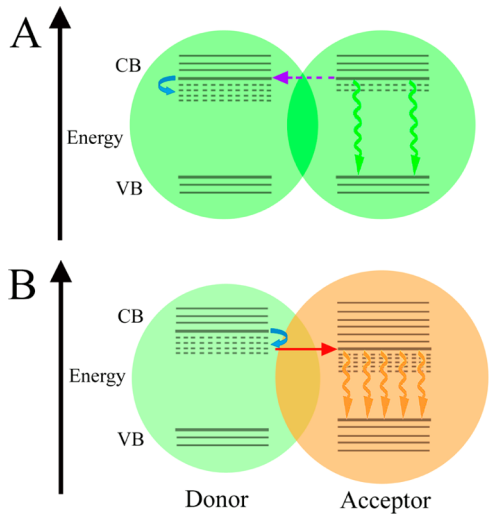

Figure 4. Illustration of the excitonic energy levels of the (A) QDs1 bilayers and (B) QDs1/QDs2 bilayers. The thick lines represent the bottom of the exciton band, thin solid lines the vibronic progressions, and the dotted lines symbolize trap states.

dx.doi.org/10.1021/ac500351d | Anal. Chem. 2014, 86, 3284−3290

trapped excitons and the efficient passing of energy could effectively funnel energy from QDs1 to QDs2, thus greatly enhancing the ECLRET efficiency and also the ECL signal. This graded-gap QD system, with quite high ECL intensity, was then implemented in the fabrication of an ECL immunosensor.

Characterization of the ECL Immunosensor. The graded-gap QD system was investigated in terms of its ECL stability. The ECL emission under consecutive potential scans from 0 to −1.5 V for 19 cycles is shown in Figure S3 of the Supporting Information. The ECL signals were high and stable, suggesting that the system is suitable for use as an ECL immunosensor.

ECL signals at each immobilization step were recorded to monitor the fabrication of the immunosensor. As shown in Figure 5A, the bare GCE exhibited only a negligible ECL signal.

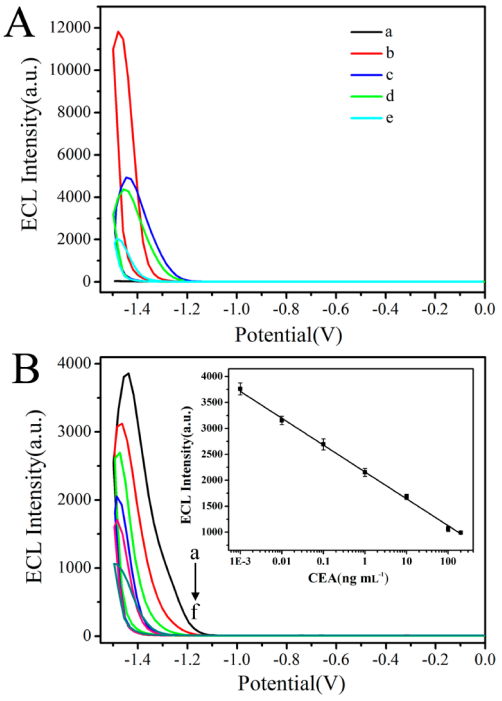

Figure 5. (A) ECL−potential curves of stepwise modified electrodes: (a) bare GE, (b) CS/QDs2/QDs1/CS/GCE, (c) Ab/CS/QDs2/QDs1/CS/GCE, (d) BSA/Ab/CS/QDs 2/QDs1/CS/GCE, and (e) Ag/BSA/Ab/CS/QDs2/QDs1/CS/GCE, where CEA concentration here is 1 ng mL^{-1}. (B) ECL potential curves of the immunosensor in the presence of (a−f) 0.001, 0.01, 0.1, 1, 10, 100 ng mL^{-1} CEA. Inset: calibration curve for CEA determination.

After modification with the CS/QDs1/QDs2/CS layers, the ECL peak intensity increased over 400-fold, which we attribute to the reaction between QDs and $S_2O_8^{2-}$ as well as to the system's highly efficient ECLRET. After rat anti-CEA (Ab) was deposited onto the GCE, the ECL signal became weaker, which can be ascribed to the insulation and steric hindrance of the conjugated proteins. The subsequent depositions of BSA and CEA (1 ng mL^{-1}) also observably decreased the ECL signal. The ECL intensity was strongly dependent on the quantity of adsorbed CEA; thus, CEA could be quantitatively determined.

ECL Detection of CEA. Figure 5B shows the ECL intensity of the immunosensor at different concentrations of CEA. The ECL intensity decreased gradually with increasing concentrations of CEA, because the specific binding of CEA with rat anti-CEA via immunoreaction greatly inhibited the ECL reaction of the material on the electrode, thus decreasing the ECL intensity. These results suggest that the CEA concentration can be determined by the ECL measurement of the immunosensor. The standard calibration curve for CEA detection is shown in the inset of Figure 5B. The ECL intensity decreased linearly with the logarithmic CEA concentration from 1 pg mL^{-1} to 200 ng mL^{-1}, with a detection limit of 0.4 pg mL^{-1}. The linear equation is I = 2160−518 log C (where C is in ng mL^{-1}), and the correlation coefficient is 0.995, thus demonstrating that we can quantitatively detect CEA concentrations.

Selectivity, Reproducibility, and Stability of the Immunosensor. To investigate the selectivity of the proposed immunosensor, we compared the ECL signal response to CEA at a concentration of 100 pg mL^{-1}, with responses to the other three interfering proteins: interleukin- 6 (IL-6), prostate specific antigen (PSA), and matrix metalloproteinase-9 (MMP-9), each at a concentration of 1 ng mL^{-1}. As shown in Figure 6A, the proposed CEA immunosensor did not show

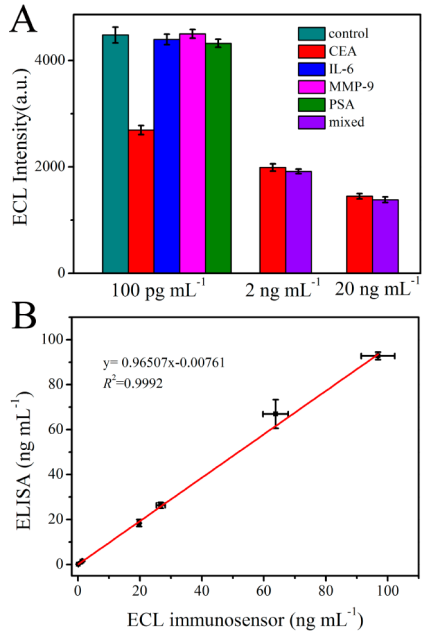

Figure 6. (A) The specificity of the ECL immunosensor toward other proteins (IL-6, MMP-9, PSA, and the mixed sample); the concentrations of interfering proteins are ten times higher than that of CEA. The control value represents ECL intensity of the immunosensor after being incubated in pure PBS under the same condition. (B) The correlation response plot between the immunosensor and ELISA methods for the determination of CEA in human serum samples.

any significant responses for other proteins as compared to the result obtained from the control experiment. Furthermore, the mixed samples, containing mixture of CEA (2 or 20 ng mL^{-1}) and all three interfering proteins (with concentrations ten times higher than that of CEA), showed no significant difference in ECL intensity from that observed for the sample containing only CEA. These results reveal that the proposed immunosensor has acceptable selectivity with minor interferences from nonspecific adsorption of other proteins.

The reproducibility of the immunosensor for CEA detection was investigated through intra- and interassay precision tests, which were conducted by measuring the same CEA sample in

dx.doi.org/10.1021/ac500351d | Anal. Chem. 2014, 86, 3284−3290

Table 1. Assay Results of Real Sera Sample by Using the ELISA and the Proposed ECL Methods

	ECL immunoassay		ELISA			
sample no.	C_{CEA} (ng mL^{-1})[a]	RSD (%)	C_{CEA} (ng mL^{-1})[a]	RSD (%)	t_{exptl}	P
1	26.74 ± 1.41	5.3	26.34 ± 1.51	1.5	0.361	0.736
2	63.80 ± 4.07	6.4	66.91 ± 6.39	4.6	0.711	0.516
3	96.83 ± 5.41	5.6	92.74 ± 1.68	4.4	1.253	0.278
4	19.76 ± 0.38	1.9	18.42 ± 1.57	7.3	1.443	0.223
5	0.15 ± 0.01	6.7	0.14 ± 0.01	10.1	1.731	0.158
6	1.34 ± 0.10	7.3	1.44 ± 0.11	5.5	0.911	0.414

[a]Analyses were made in triplicate, and the data were obtained as mean values of three assays (n = 3).

triplicate and by measuring CEA with three separate immunosensor assemblies fabricated on the same electrode. The intra- and interassay RSDs for 1 ng mL^{-1} CEA were 4.2% and 3.5%, respectively, indicating that the immunosensor had acceptable precision and fabrication reproducibility.

After the immunosensor was stored in pH 7.4 PBS at 4 °C for 20 days, no significant change was observed in its analytical performance for the same CEA concentration, which indicated that the immunosensor had good stability.

Analysis of Real Samples and Evaluation of Method Accuracy. The analytical reliability and potential applicability of the immunoassay for clinical applications was evaluated by comparing the assay results of clinical serum samples using the proposed ECL immunosensor with those obtained by using the commercially available human CEA enzyme-linked immunosorbent assay (ELISA) kit. We examined six human serum samples, among which two were in the normal CEA levels (0–10 ng mL^{-1}) and the other four were higher than 10 ng mL^{-1}. Taking into consideration the normal CEA levels and the linear response range of our method, the samples did not need to be diluted in advance. The assay results are listed in Table 1. Statistical analysis of the experimental results was performed by using a t test between two methods. As shown in Table 1, the t_{exptl} values in all cases were below t_{crit} ($t_{crit}[4, 0.05] = 2.77$)[47] and the P values [Sig.(2-tailed)] were all more than 0.05. In addition, comparison of the experimental results using the proposed ECL immunoassay with those by the ELISA method was performed via linear regression analysis (Figure 6B). The slope and intercept of the regression equation were 0.965 ± 0.013 and −0.008 ± 0.008, respectively, close to the ideals of "1" and "0".[48] These results obviously show that there is no significant difference between the results obtained by the ECL and ELISA methods. Thus, the developed immunosensor can be satisfactorily applied to the clinical determination of CEA levels in human serum.

CONCLUSIONS

In conclusion, we have demonstrated that an integrated system relying on ECLRET-based energy funneling in graded-gap QD bilayers enabled sensitive analysis of CEA with a high degree of reliability. The recycling effect of trapped excitons, as well as the stepwise passing of excitation energy, markedly enhanced the ECL intensity. Furthermore, the intense ECL signal obtained from the graded-gap QD system made the system a promising candidate for the development of a sensitive ECL immunosensor. The developed immunosensor has been successfully applied to the detection of CEA in a human serum sample, and the results were validated by using the conventional ELISA method and showed high consistency. The observed ECL enhancement effect in graded-gap QD bilayers paves the way for further studies of ECL energy transfer cascades in QD multilayers. This work also opens new avenues to employ graded-gap QD systems as novel platform for sensitive detection of various biomolecules.

ASSOCIATED CONTENT

Supporting Information

Additional information as noted in text. This material is available free of charge via the Internet at http://pubs.acs.org.

AUTHOR INFORMATION

Corresponding Authors

*E-mail: lll-100@163.com. Tel/Fax: +86-25-83597204.
*E-mail: jjzhu@nju.edu.cn.

Notes

The authors declare no competing financial interest.

ACKNOWLEDGMENTS

The authors thank the National Basic Research Program of China (Grant 2011CB933502) and the National Natural Science Foundation of China (Grants 21103088, 21335004, and 21121091) for financial support. This work is also supported by the Postdoctoral Science Foundation of China (Grants 2012M521039 and 2013T60522) and Jiangsu Planned Projects for Postdoctoral Research Funds (Grant 1201001B).

REFERENCES

(1) Harma, H.; Soukkab, T.; Shavel, A.; Gaponikd, N.; Weller, H. *Anal. Chim. Acta* **2007**, *604*, 177–183.
(2) Wang, S.; Mamedova, N.; Kotov, N. A.; Chen, W.; Studer, J. *Nano Lett.* **2002**, *2*, 817.
(3) Kagan, C. R.; Murray, C. B.; Nirmal, M.; Bawendi, M. G. *Phys. Rev. Lett.* **1996**, *76*, 1517.
(4) Franzl, T.; Koktysh, D. S.; Klar, T. A.; Rogach, A. L.; Feldmann, J.; Gaponik, N. *Appl. Phys. Lett.* **2004**, *84*, 2904.
(5) Zhang, C. Y.; Johnson, L. W. *Anal. Chem.* **2006**, *78*, 5532.
(6) Nikiforov, T. T.; Beechem, J. M. *Anal. Biochem.* **2006**, *357*, 68.
(7) Franzl, T.; Shavel, A.; Rogach, A. L.; Gaponik, N.; Klar, T. A.; Eychmuller, A.; Feldmann, J. *Small* **2005**, *1*, 392–395.
(8) Guo, L.; Krauss, T. D.; Poitras, C. B.; Lipson, M.; Teng, X.; Yang, H. *Appl. Phys. Lett.* **2006**, *89*, 061104–3.
(9) Clark, S. W.; Harbold, J. M.; Wise, F. W. *J. Phys. Chem. C* **2007**, *111*, 7302–7305.
(10) Carriba, P.; Navarro, G.; Ciruela, F.; et al. *Nat. Methods* **2008**, *5*, 727–733.
(11) Lee, J. S.; Joung, H.-A.; Kim, M.-G.; Park, C. B. *ACS Nano* **2012**, *6*, 2978–2983.
(12) Wu, M. S.; Shi, H. W.; Xu, J. J.; Chen, H. Y. *Chem. Commun.* **2011**, *47*, 7752–7754.
(13) Hu, L. Z.; Xu, G. B. *Chem. Soc. Rev.* **2010**, *39*, 3275–3304.
(14) Miao, W. J. *Chem. Rev.* **2008**, *108*, 2506–2553.
(15) Richter, M. M. *Chem. Rev.* **2004**, *104*, 3003–3036.

(16) Forster, R. J.; Bertoncello, P.; Keyes, T. E. *Annu. Rev. Anal. Chem.* **2009**, *2*, 359−385.
(17) Xu, S.; Liu, Y.; Wang, T.; Li, J. *Anal. Chem.* **2011**, *83*, 3817−3823.
(18) Shen, M.; Xu-Hui Zhu, X.-H.; Bard, A. J. *J. Am. Chem. Soc.* **2013**, *135*, 8868−8873.
(19) Cheng, C.; Huang, Y.; Wang, J.; Zheng, B.; Yuan, H.; Xiao, D. *Anal. Chem.* **2013**, *85*, 2601−2605.
(20) Sardesai, N. P.; Barron, J. C.; Rusling, J. F. *Anal. Chem.* **2011**, *83*, 6698−6703.
(21) Wu, L.; Wang, J.; Ren, J.; Li, W.; Qu, X. G. *Chem. Commun.* **2013**, *49* (5), 675−5677.
(22) Zhou, H.; Zhang, Y.-Y.; Liu, J.; Xu, J.-J.; Chen, H.-Y. *Chem. Commun.* **2013**, *49*, 2246−2248.
(23) Zou, G. Z.; Ju, H. X. *Anal. Chem.* **2004**, *76*, 6871−6876.
(24) Zou, G. Z.; Ju, H. X.; Ding, W. P.; Chen, H. Y. *J. Electroanal. Chem.* **2005**, *579*, 175−180.
(25) Ding, S. N.; Xu, J. J.; Chen, H. Y. *Chem. Commun.* **2006**, 3631−3633.
(26) Kang, J. Z.; Wei, H.; Guo, W. W.; Wang, E. K. *Electrochem. Commun.* **2007**, *9*, 465−468.
(27) Alivisatos, A. P. *Science* **1996**, *271*, 933.
(28) Li, L. L.; Shen, Y. Y.; Xu, M.; Ji, J.; Lu, Q.; Fei, R.; Zhang, K.; Zhang, J. R.; Zhu, J. J. *Sci. Rep.* **2013**, *3*, 1529.
(29) Biju, V.; Anas, A.; Akita, H.; Shibu, E. S.; Itoh, T.; Harashima, H.; Ishikawa, M. *ACS Nano* **2012**, *6*, 3776−3788.
(30) Lin, Y. W.; Tseng, W. L.; Chang, H. T. *Adv. Mater.* **2006**, *18*, 1381−1386.
(31) Liang, R.; Xu, S.; Yan, D.; Shi, W.; Tian, R.; Yan, H.; Wei, M.; Evans, G. D.; Duan, X. *Adv. Funct. Mater.* **2012**, *22*, 4940−4948.
(32) Santra, P. K; Kamat, P. V. *J. Am. Chem. Soc.* **2013**, *135*, 877−885.
(33) Choi, S.; Jin, H.; Bang, J.; Kim, S. *J. Phys. Chem. Lett.* **2012**, *3*, 3442−3447.
(34) Ruland, A.; Schulz-Drost, C.; Sgobba, V.; Guldi, D. M. *Adv. Mater.* **2011**, *23*, 4573−4577.
(35) Klar, T. A.; Franzl, T.; Rogach, A. L.; Feldmann, J. *Adv. Mater.* **2005**, *17*, 769−773.
(36) Franzl, T.; Klar, T. A.; Schietinger, S.; Rogach, A. L.; Klar, T. A.; Feldmann, J. *Nano Lett.* **2004**, *4*, 1599−1603.
(37) Boulesbaa, A.; Issac, A.; Stockwell, D.; Huang, Z.; Huang, J.; Guo, J.; Lian, T. *J. Am. Chem. Soc.* **2007**, *129*, 15132−15133.
(38) Funston, A. M.; Jasieniak, J. J.; Mulvaney, P. *Adv. Mater.* **2008**, *20*, 4274−4280.
(39) Dayal, S.; Lou, Y.; Samia, A. C. S.; Berlin, J. C.; Kenney, M. E.; Burda, C. *J. Am. Chem. Soc.* **2006**, *128*, 13974−13975.
(40) Wargnier, R.; Baranov, A. V.; Maslov, V. G.; Stsiapura, V.; Artemyev, M.; Pluot, M.; Sukhanova, A.; Nabiev, I. *Nano Lett.* **2004**, *4*, 451−457.
(41) Shen, Y. Y.; Li, L. L.; Lu, Q.; Ji, J.; Fei, R.; Zhang, J. R.; Abdel-Halimb, E. S.; Zhu, J. J. *Chem. Commun.* **2012**, *48*, 2222−2224.
(42) Clapp, A. R.; Medintz, I. L.; Mauro, J. M.; Fisher, B. R.; Bawendi, M. G.; Mattoussi, H. *J. Am. Chem. Soc.* **2004**, *126*, 301−310.
(43) Jie, G. F.; Li, L. L.; Chen, C.; Xuan, J.; Zhu, J. J. *Biosen. Bioelectron.* **2009**, *24*, 3352−3358.
(44) Zheng, L. Y.; Chi, Y. W.; Dong, Y. Q.; Lin, J. P.; Wang, B. B. *J . Am. Chem. Soc.* **2009**, *131*, 4564.
(45) Santra, P. K; Kamat, P. V. *J. Am. Chem. Soc.* **2013**, *135*, 877−885.
(46) Liang, R. Z.; Xu, S. M.; Yan, D. P.; Shi, W. Y.; Tian, R.; Yan, H.; Wei, M.; Evans, D. G.; Duan, X. *Adv. Funct. Mater.* **2012**, *22*, 4940−4948.
(47) Zhang, B.; Tang, D. P.; Goryacheva, I. Y.; Niessner, R.; Knopp, D. *Chem.—Eur. J.* **2013**, *19*, 2496−2503.
(48) Tang, D. P.; Liu, B. Q.; Niessner, R.; Li, P. W.; Knopp, D. *Anal. Chem.* **2013**, *85*, 10589−10596.